ANEURYSM NECK OVERESTIMATION HAS A RELATIVELY MODEST IMPACT ON SIMULATED HEMODYNAMICS*

Daniel E. MacDonald[1], Nicole M. Cancelliere[2], Vitor M. Pereira[2, 3], and David A. Steinman[1]

[1]Biomedical Simulation Lab, Department of Mechanical & Industrial Engineering
University of Toronto, Toronto, Ontario, Canada
[2]RADIS Lab, Li Ka-Shing Knowledge Institute, St. Michael's Hospital
University of Toronto, Toronto, Ontario, Canada
[3]Division of Neurosurgery, Department of Surgery, St. Michael's Hospital
University of Toronto, Toronto, Ontario, Canada

ABSTRACT

Overestimation of intracranial aneurysm neck width by 3D angiography is a recognized clinical problem and has long been a concern for image-based computational fluid dynamics (CFD). Recently, it was demonstrated that neck overestimation in 3D rotational angiography (3DRA) could be corrected via segmentation with upsampled resolution and gradient enhancement (SURGE). Our aim was to determine whether and how such corrections would impact CFD-derived hemodynamics. A subset of 17 cases having the largest neck errors from a consecutive clinical sample of 60 was segmented from 3DRA using both standard watershed and SURGE methods. High-fidelity, pulsatile CFD was performed, from which were derived a variety of scalar hemodynamic parameters thought to be associated with aneurysm growth and/or rupture status. With a few exceptions, flow and wall shear stress (WSS) patterns were qualitatively similar between Standard and SURGE-derived models. Sac-averaged WSS values were significantly lower in SURGE models (p=0.0005) but were highly correlated with their Standard counterparts (R^2=0.98). Jet impingement was significantly more concentrated in the SURGE vs. standard models (p=0.0011), and only moderately correlated (R^2=0.61). Parameters quantifying velocity or WSS fluctuations were not significantly different between models, but this reflected their poorer correlations (R^2 <0.4). Nevertheless, for all hemodynamic parameters, median absolute differences were <26%, and no parameter had more than 5 cases with absolute differences >50%. Differences were shown to be at most equal to, and often less than, those reported for other sources of error/uncertainty in intracranial aneurysm CFD, such as solver settings or assumed inflow rates.

Keywords aneurysm · CFD · segmentation · hemodynamics · flow instability

1 Introduction

In 2009, the neck width of intracranial aneurysms (hereafter, simply aneurysms) was shown to be systematically overestimated when measured from three-dimensional rotational angiography (3DRA) compared with 2D digital subtraction angiography (2D-DSA), owing to high curvature at the neck [1]. Subsequently, in 2013, it was shown that such neck overestimation might have a "non-negligible" impact on qualitative hemodynamic features derived from 3DRA-based computational fluid dynamics (CFD), such as inflow jet penetration and impingement zone [2]. Since then, many image-based aneurysm CFD studies have been performed, notably recent ones showing significant associations between inflow jet intensity, concentration and stability, and aneurysm growth and/or rupture status [3, 4].

Citation: This article has been accepted for publication in *Cardiovasc Eng Tech* 14, 252–263 (2023) following peer review, and the Version of Record can be accessed online at https://doi.org/10.1007/s13239-022-00652-0.

As highlighted in a recent review of sources of error and uncertainty in aneurysm CFD [5, 6], however, the relative importance of neck overestimation remains unclear, as does its prevalence. In the 2018 Multiple Aneurysms Anatomy Challenge (MATCH), participants consistently overestimated the neck width of one case, suggesting that a wide variety of commonly used segmentation methods are susceptible to neck overestimation; only one team accurately recovered the aneurysm neck, but reporting a manual editing time of 26 hours [7]. Even modern deep-learning segmentation methods appear susceptible to neck overestimation: in the 2020 Cerebral Aneurysm Detection and Analysis (CADA) challenge, the neck was cited as the most common and substantial region of error among top submitted solutions [8]. Neck overestimation may also be exacerbated by less-invasive-but-lower-resolution computed tomography (CT) or magnetic resonance (MR) angiography [9] upon which some aneurysm CFD models are also based.

Given the recent interest in hemodynamic parameters associated with jetting of flow into the aneurysm sac, there is a need to understand how neck overestimation (which, from basic fluid dynamic principles, can be expected to have an outsized effect on inflow jetting) might impact purported hemodynamic predictors of aneurysm growth or rupture before they can be deployed or trusted for clinical use. Towards this end, we recently showed how segmentation of 3DRA images with upsampled resolution and gradient enhancement (SURGE) could help overcome such neck overestimation [10]. In that study, we applied SURGE to N = 60 consecutive cases from a single aneurysm clinic and compared measurements of neck width by standard watershed segmentation and by gold-standard 2D-DSA. Having established the prevalence and quantitative nature of aneurysm neck overestimation, the present study now seeks to provide clarity on the impact on hemodynamic parameters, for the first time quantitatively, in a controlled manner by comparing CFD simulations derived from conventional 3DRA segmentations having neck overestimations vs. those for which those overestimations were corrected by SURGE.

2 Materials and Methods

2.1 Study cohort

This study was performed under Toronto Western Hospital's Research Ethics Board Approval 19-5823, which authorizes research analysis and publication of anonymized and de-identified patient imaging data from its aneurysm clinic. The selection criteria of the original 60 cases can be found in [10]. The initial neck measurements, which for each case were taken from a single projection matching the reference 2D-DSA image, provide an incomplete picture of potential changes of the ostium: for ostia with high eccentricity or irregular shape, a single 2D measurement may not capture differences that may be viewed from other projections. For this reason, we visually identified cases from this cohort with differences in the size, location, or definition of the neck between the standard watershed (hereafter denoted "Standard") and SURGE preliminary segmentations. We excluded cases that had differences other than the neck, for example cases where a sac-adjacent vessel could not be captured by Standard segmentation, which would result in topological differences causing inconsistency in boundary conditions. Of the final selection of cases (N = 17), the median neck error relative to 2D-DSA was 0.25 mm for SURGE, compared with 0.68 mm for Standard watershed. Aneurysm characteristics, neck widths and ostium areas for these cases are provided as electronic supplementary material[2].

2.2 Surface and volume mesh preparation

As illustrated in Fig. 1, we generated Standard and SURGE watershed segmentations for each of the 17 pairs. When performing segmentation, the watershed marker points were consistent within the aneurysm ROI for Standard and SURGE methods. Considerable care was taken to control for potential differences between the Standard and SURGE surfaces beyond the neck and sac, since these could confound any observed changes in hemodynamics. First, each case was segmented using Standard watershed, including the full parent artery and daughter branches, and a preliminary surface was generated (Fig. 1A). Basic clipping was performed on this mesh to remove extraneous vessels and to open inlets/outlets. Then, a ROI containing the aneurysm (Fig. 1B, box) was segmented using SURGE, and "pasted" into a copy of the Standard watershed surface (Fig. 1C), with MeshFix [11] being used to ensure the pasting was watertight. For each resulting pair of surfaces (Fig. 1D and Fig. 1E) subsequent operations (surface remeshing and smoothing, flow extensions, volume meshing) were identically performed using the Vascular Modelling ToolKit (VMTK) [12].

Flow extensions were added using VMTK with a length of 4 diameters. A prismatic boundary layer comprising 4 sublayers was imposed at the wall, with total thickness equal to 85% of the local mesh tetrahedron edge length and sublayer thickness decreasing by 25% for each layer. The aneurysm and perianeurysmal region were meshed using tetrahedral elements with a uniform edge length of 0.15 mm, previously shown to be sufficient for capturing flow instabilities [13]. Throughout the rest of the model, edge length varied in proportion to local vessel radius and

[2]https://figshare.com/s/9b52dd83a6c860172fa1

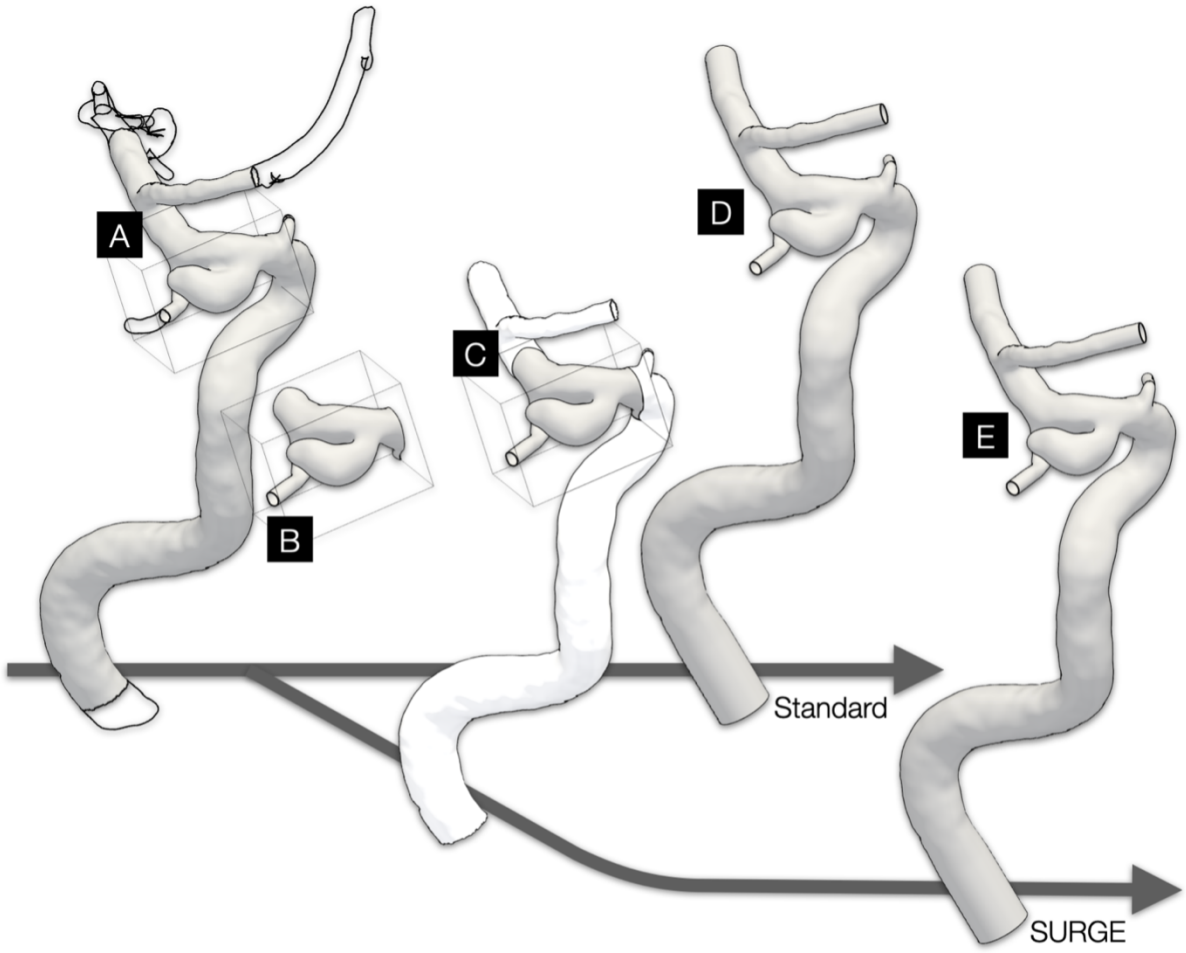

Figure 1: Illustration of the mesh preparation strategy. (A) A preliminary surface was generated for the Standard watershed segmentation, demonstrating neck overestimation, and basic clipping was performed to open inlets/outlets; (B) a surface was generated using the SURGE method for the aneurysm ROI; (C) the local segmentation from the SURGE ROI is "pasted" into a copy of the Standard surface; (D) the Standard surface was smoothed and flow extensions were added; (E) The merged SURGE surface was identically processed.

curvature, with upper and lower bounds of 0.4 mm and 0.15 mm. The median number of elements and nodes was 2.2 million and 350,000, respectively, and with node densities in the sacs ranging from 700-1000 nodes/mm^3. Mesh quality was ensured using recommended settings of the underlying Tetgen engine [14] and by inspection of mesh quality indices [15].

The mean number of elements per mesh was 2.2 million.

2.3 CFD simulation

Patient-specific flow rates were not available for these cases, so we used a previously described and validated methodology [16]. A fully-developed pulsatile (Womersley) velocity profile was imposed at the model inlet using a waveform based on older adults. Individual flow rates were calculated such that time-averaged inlet velocity was 27 cm/s for each case. Outlet flow was prescribed according to a flow splitting-scheme based on cross-sectional areas and enforced as traction-free boundary conditions [17].

Simulations were performed using the well-validated, minimally dissipative finite-element CFD solver Oasis [18] using linear (P1-P1) elements. Simulations were run for 2 cardiac cycles of period 0.951 s with 9600 timesteps per

Table 1: Hemodynamic parameters evaluated for the Standard and SURGE groups.

Parameter	Description ([] indicates units for dimensional parameters)
Qin	Ostium inflow rate [cm^3/s]
TAWSS	Time-averaged wall shear stress (WSS), spatially averaged over the sac [Pa]
OSI	Oscillatory shear index
RRT	Relative residence time, spatially averaged over the sac [Pa^{-1}]
LSA	Low shear area, the proportion of the sac exposed to low WSS, averaged over the cardiac cycle
ICI	Inflow concentration index, the degree of concentration of the flow stream entering the sac, averaged over the cardiac cycle
SCI	Shear concentration index, the degree of concentration of high WSS on the sac, averaged over the cardiac cycle
SPI	Spectral power index, the relative power of high-frequency temporal fluctuations in velocity magnitude
SBI	Spectral bandedness index, a measure of whether velocity magnitude fluctuations are broad-banded, suggesting turbulent-like flow, or narrow-banded, suggesting vortex-shedding or other intra-cycle periodicities

cycle. Snapshots of the flow were saved every 10th timestep, resulting in a sampling frequency of $\sim$1 kHz. Blood viscosity and density were assumed to be 3.7 mPa-s and 1.06 kg/m3.

2.4 Statistical analysis

We hypothesized that the neck changes introduced by SURGE would result in statistically different measurements of various reported hemodynamic parameters, described in Table 1. All parameters except RRT, SPI, and SBI are defined in [19]; RRT is defined in [20], SPI in [21] and SBI in [4]. These parameters were chosen because they are commonly used; they quantify neck-related features such as jet concentration; and/or they have been associated with aneurysm growth or rupture [3, 22, 23].

All parameters were found to follow non-normal distributions as determined by Shapiro-Wilk tests, so we performed pairwise comparisons using the two-sided Wilcoxon signed-rank test. Linear regressions were performed to evaluate correlations of Standard vs. SURGE CFD-derived hemodynamic parameters, and correlations between ostium errors and hemodynamic differences.

3 Results

Of the 17 aneurysms, 12 were at bifurcations and 5 were sidewall type, and located at the internal (7), anterior (7) or middle (2) cerebral arteries (ICA, ACA, MCA, respectively), and 1 at the basilar artery. The median aneurysm size was 5.21 mm. The median neck diameter for the Standard and SURGE groups was 4.27 mm and 3.54 mm, respectively. The median difference in ostium area between Standard and Surge segmentations was 1.4 mm^2, with a maximum difference of 6.6 mm^2.

Fig. 2 shows representative examples of 3D surfaces and hemodynamics from this dataset. Comparisons for each case (A-Q) individually are available as electronic supplementary material[3]. In most cases (A, B, D, G, H), the inflow jet of the Standard group penetrates further into the sac compared with the SURGE group, suggesting higher jet velocities, though a counter example is also present (case F). TAWSS is generally highest in regions near the ostium, near jet impingement zones, and (as in cases D and H) in regions where the jet enters the sac along the wall. The qualitative distributions of TAWSS are generally similar between pairs, with a few exceptions: for example, in case A, the jet is more coherent in the SURGE model, and impingement is observed near the top of the sac, whereas the Standard model has a high-shear zone all along the left side of the aneurysm. Unlike TAWSS, clear and apparent differences are found in instantaneous flow structures, visualized here using Q-criterion, highlighting the complex spatiotemporal differences between pairs. We show sac-average spectrograms generated as in [24] to illustrate high-frequency flow instabilities through the cardiac cycle. All cases except for D show similar spectral power and characteristics between the pairs, suggesting similar levels of flow instability.

To quantitatively assess differences in flow, we present regression plots of Standard vs. SURGE CFD-derived hemodynamic parameters in Fig. 3, and summary statistics of the hemodynamic parameters and their percentage differences are provided in Tables 2 and 3, respectively. Hemodynamic parameters for all cases are provided as electronic supplementary material[4].

[3] https://figshare.com/s/8d03649dd56f55ce385e
[4] https://figshare.com/s/9b52dd83a6c860172fa1

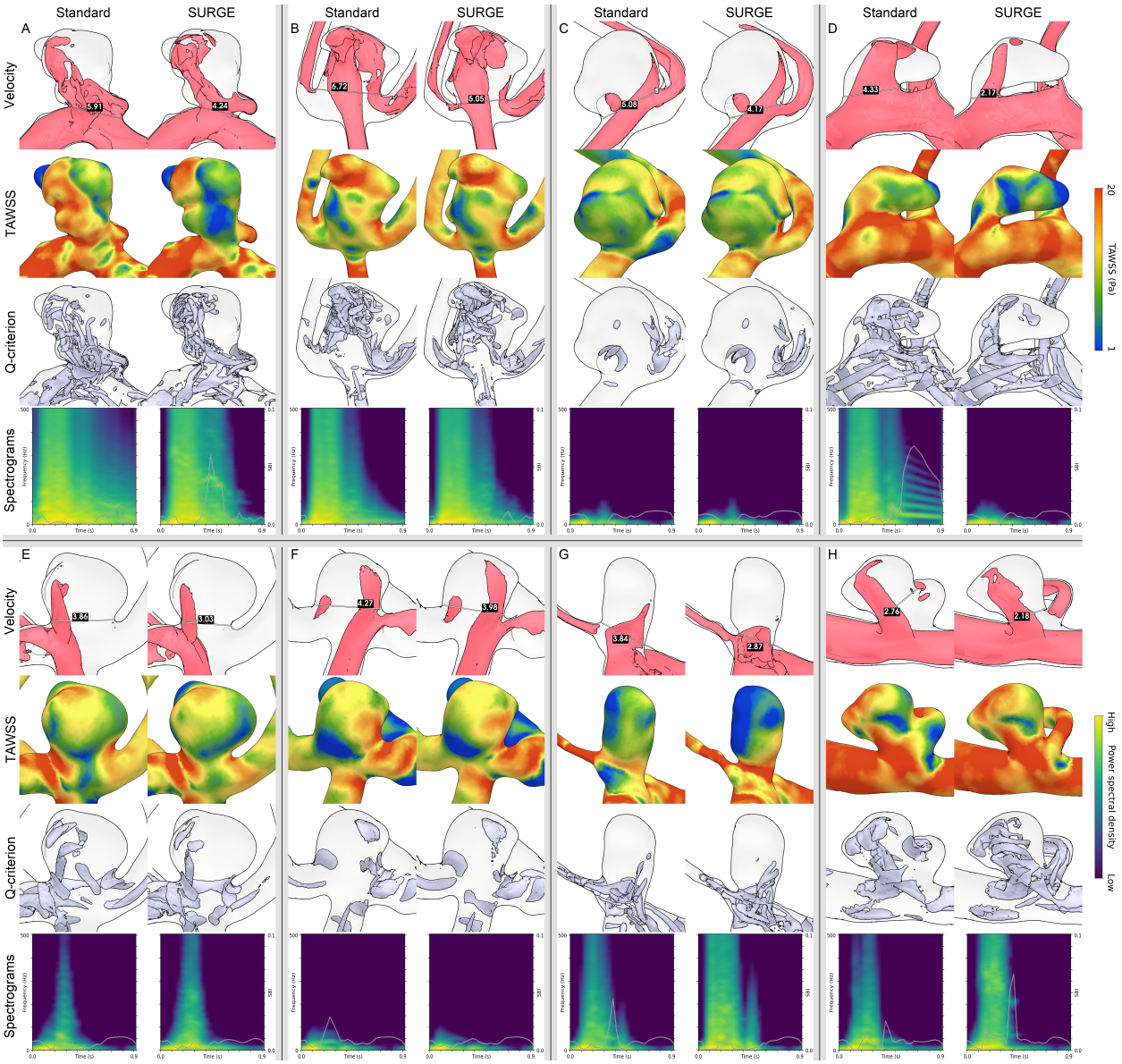

Figure 2: Comparison of surfaces and hemodynamics for 8 representative cases. Neck measurements are presented in millimeters. Velocity magnitude (0.75 m/s) and Q-criterion (0.5) contours were generated at t = 0.19 s. TAWSS is presented on a logarithmic scale, as are the sac-averaged spectrograms.

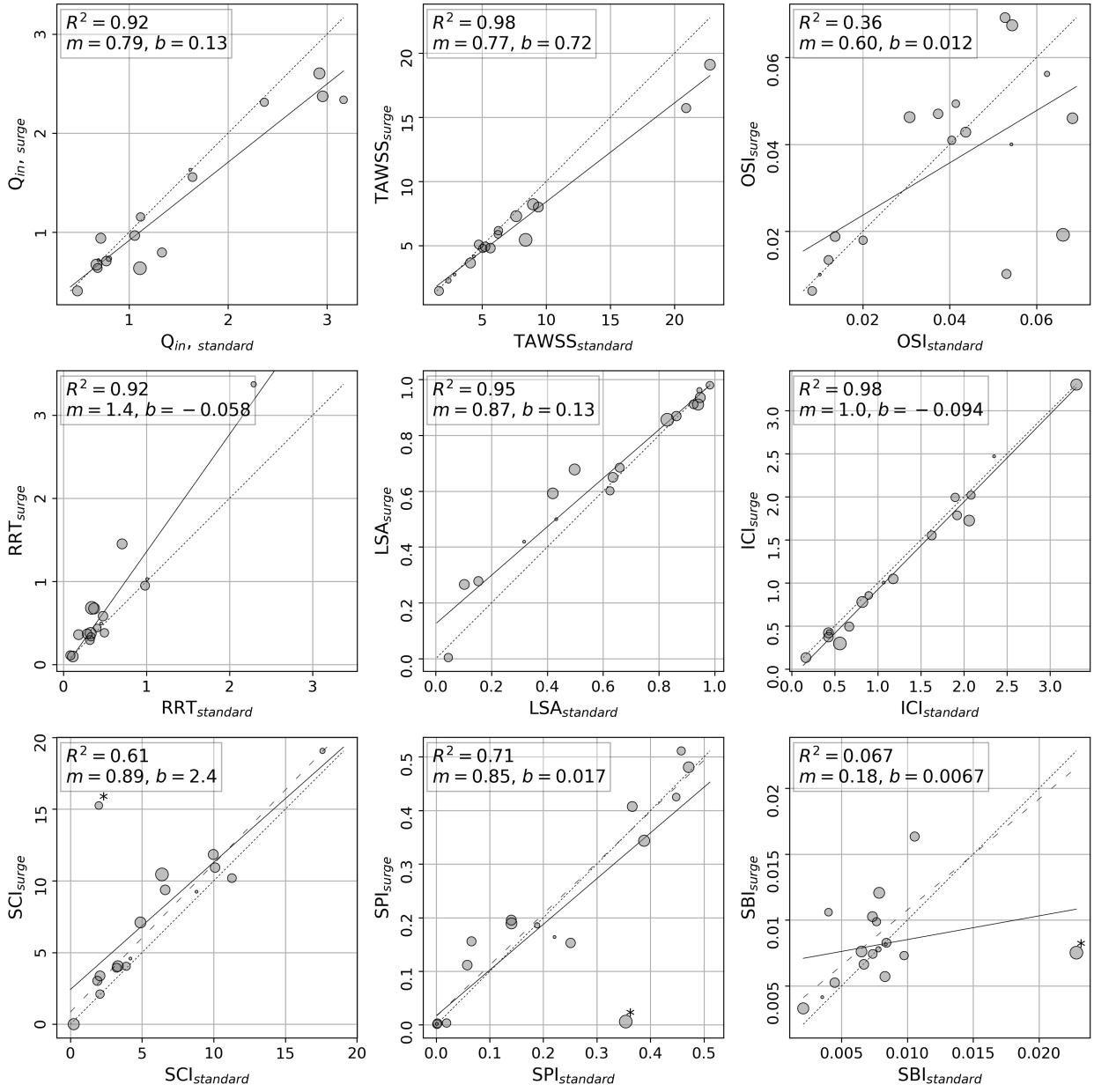

Figure 3: Correlation plots of hemodynamic parameters extracted from paired CFD simulations using 3D models generated using Standard watershed segmentation (x-axis) vs SURGE segmentation (y-axis). Marker area is proportional to the change in neck area. R^2 is the coefficient of determination, m and b indicate the slope and intercept of the line of best fit. The dotted diagonal lines have slope of 1 and the solid line indicates the line of best fit using simple linear regression. For SCI, SPI, and SBI, we indicate potential outlier points with (*) and plot lines of best-fit with these points removed using the dashed line.

Table 2: Descriptive statistics of hemodynamic parameters extracted from paired CFD simulations of aneurysm models generated using Standard watershed segmentation vs. SURGE segmentation.

	Standard		SURGE		Difference*	
	Median	IQR	Median	IQR	W	p-value
Qin	1.11	0.71–1.64	0.94	0.71 – 1.63	22	0.0079
TAWSS	5.65	4.37–8.40	5.09	4.17 – 7.30	9	0.0005
OSI	0.041	0.020–0.054	0.041	0.018 – 0.047	70	0.78
RRT	0.37	0.32 – 0.50	0.44	0.36 – 0.68	25	0.013
LSA	0.64	0.42 – 0.92	0.68	0.50 – 0.91	36	0.057
ICI	1.07	0.56 – 1.92	1.01	0.43 – 1.78	23	0.0093
SCI	4.19	2.07 – 8.81	7.1	3.94 – 10.45	12	0.0011
SPI	0.19	0.058 – 0.37	0.16	0.0061 – 0.34	74	0.93
SBI	0.0077	0.0065 – 0.0084	0.0076	0.0066 – 0.0099	53	0.28

*Shown are the test statistics, W, and p-values for the paired two-sided Wilcoxon signed-rank test for differences between Standard- and SURGE-derived hemodynamic parameters.

Table 3: Descriptive statistics of percentage differences extracted from paired CFD simulations of aneurysm models generated using Standard watershed segmentation vs. SURGE segmentation.

	Median	|P25|	|P50|	|P75|	|Max|
Qin	-8.0%	3.90%	8.10%	20%	43%
TAWSS	-6.20%	4.70%	7.40%	15%	35%
OSI	-0.51%	10%	25%	33%	81%
RRT	15%	7.90%	22%	47%	110%
LSA	2.3%	1.70%	3.70%	36%	160%
ICI	-5.0%	4.30%	5.10%	13%	47%
SCI	19%	8.30%	22%	61%	670%
SPI	2.0%	11%	26%	53%	140%
SBI	17%	2.4%	25%	54%	160%

Median indicates the median (signed) percentage difference; Pn indicates the n^{th} percentile of absolute percentage difference; and Max indicates the maximum absolute percentage difference.

The average flow rate entering the aneurysm (Q_{in}) was lower in the SURGE cohort (median = 8%) but showed strong correlation (R^2 = 0.92). This reduction in aneurysm flow rate agrees with the general reduction in jet penetration in Fig. 2. Like Q_{in}, sac TAWSS was statistically lower in the SURGE group ($p < 0.001$), showing a decrease in 16/17 cases. The median change was -6.2% and the greatest change was -35%, but otherwise they were strongly correlated (R^2 = 0.98). In contrast to the apparent stability of TAWSS with neck segmentation errors, OSI showed high sensitivity to neck changes with a median absolute difference of 25% and a maximum change of 81%. No clear trend of over- vs underestimation was evident, as suggested by the low R^2 = 0.36. RRT was statistically higher in the SURGE group, with a median difference of +15% and 13/17 cases showing an increase. Given that RRT is derived from TAWSS and OSI, it is reasonable that the trend and significance is a balance of the two parameters, i.e., if TAWSS tends to be reduced by SURGE, RRT should be increased; and the additional scatter of OSI is manifested in the additional scatter of RRT. LSA tended to be slightly higher in the SURGE group (11/17 higher) with a mean change of +2.3% and mean absolute change of 3.7%, but this difference was not strictly significant between the two groups (p = 0.057). The correlation of LSA was slightly lower than TAWSS (R^2 = 0.95 vs 0.98), but the slope of LSA was closer to 1 (0.87 vs. 0.77), suggesting LSA may be less sensitive to changes at the neck because it is a normalized parameter.

We expected ICI to be sensitive to neck segmentation since it incorporates various ostium characteristics (ICI = (Q_{in} / Q_{parent}) / (A_{in} / A_{ostium})), but our results indicate that ICI was surprisingly robust to change, exhibiting a slight decrease in the narrower-necked SURGE group (p = 0.01), with a median change of -5%, and a maximum absolute change of 47%. The slope of the line of best fit was 1.0 with R^2 = 0.98, indicating agreement between Standard and SURGE cohorts, but with a slight negative bias. Since Q_{parent} does not change between each Standard and SURGE pair, this suggests that the reduction in Q_{in} is compensated by a proportional decrease in the area ratio (A_{in} / A_{ostium}).

Although ICI was slightly lower in SURGE segmentations, suggesting less concentrated inflow (relative to ostium area), SCI was higher in 15/17 cases, with a median change of +19%, suggesting more-concentrated regions of shear

Table 4: Correlations for SCI, SPI, SBI with a potential "outliers" omitted.

	Slope	Intercept	R^2
SCI	1.0	0.85	0.93
SPI	0.96	0.016	0.92
SBI	0.84	0.0023	0.37

For SCI, we exclude case A. For SPI and SBI, we exclude case D.

Table 5: Coefficients for linear regression of absolute percentage difference in ostium area between Standard and SURGE models vs. absolute percentage difference in each hemodynamic parameter.

	Slope	Intercept	R^2
Qin	0.81	6.4	0.31
TAWSS	0.54	2.9	0.5
OSI	1.2	10	0.34
RRT	1.9	8.8	0.33
LSA	-0.059	29	0.00023
ICI	0.67	0.98	0.42
SCI	-0.95	81	0.0046
SPI	0.88	27	0.061
SBI	0.81	23	0.051

A slope of 1 indicates that a 100% increase in ostium area was associated with a 100% increase in a given hemodynamic parameter

on the aneurysm wall. In accordance with our observed reduction in Q_{in}, this may imply a weakened jet reduces the impact zone of high-shear stress on the sac, thereby increasing shear concentration. A potentially anomalous (but also explanatory) data point (case A in Fig. 2) exhibiting an SCI increase of 670% (from 1.98 to 15.25) was also observed. The jet is more concentrated in the SURGE case, resulting in a high-concentration impingement zone in the TAWSS field, supporting the reported value of SCI.

SPI showed some sensitivity to changes at the neck with no clear trends and a median absolute difference (26%) and a maximum difference of 140%. This supports our expectation that measures of flow complexity (such as the vortical Q-criterion structures in Fig. 2) are likely more sensitive to changes in geometry. Similarly, SBI showed sensitivity to neck changes with a median absolute difference of 25% and no clear trends found. The case that demonstrated the greatest change in both SPI and SBI also demonstrated the greatest change in ostium area (6.6 mm2 or 46%), visualized in Fig. 2D, where differences in the spectrogram are also clearly apparent. As shown in Fig. 3, for SCI, SPI, and SBI, the relatively low correlations may each be driven by a single influential point; in Table 4, we provide summaries of correlations with these extrema removed, which we discuss later. It should also be noted that in Fig. 3, the marker size is proportional to the percent change in neck area, yet marker size does not appear to strongly correlate, at least visually, with changes in hemodynamics, suggesting that even small changes to the neck can impact hemodynamic parameters. Per the linear regression results shown in Table 5, absolute value of percent change in TAWSS shows the strongest correlation with percent change in ostium area (R^2 = 0.50), followed by OSI, RRT, and Q_{in}; all other parameters had $R^2 < 0.1$, with LSA having near-zero correlation ($R^2 < 0.001$).

4 Discussion

Using the newly proposed SURGE method, we have shown the impact of neck segmentation on a variety of hemodynamic parameters. The narrower-neck SURGE group saw a reduction in aneurysm inflow, resulting in significant differences in various hemodynamic parameters. This may be explained by the fact that narrower necks can be expected to offer greater flow resistance, leading to lower velocities within the sac. Measures of flow spatiotemporal complexity (OSI, SPI, SBI, and to some degree SCI) appear especially sensitive to changes in ostium geometry. Neck overestimation has previously been discussed in the context of imaging [1] and qualitative differences in CFD [2], but quantitative assessment of the impact on CFD has so far been limited.

4.1 Relationship to previous studies of neck/segmentation errors

Previously, [2] demonstrated the importance of neck segmentation on CFD-derived hemodynamic parameters; in a cohort of N = 20 cases, 8/20 segmentations generated from 3DRA had overestimated necks relative to 2D-DSA. The authors manually edited the N = 8 segmentations to match 2D-DSA, resulting in an average ostium area reduction of 19%. Using qualitative ratings by two observers, they identified changes in the location and size of the inflow jet (2/8), impingement zone (3/8), and size of the low WSS zone (4/8), supporting the notion that neck overestimation can have "non-negligible" consequences on the CFD results. Our study extends this research to assess the sensitivity of common quantitative hemodynamic parameters to segmentation-induced neck changes in a cohort of N = 17 aneurysms using a semi-automated segmentation method. Our results are in-line with Schneiders et al., with a median ostium area reduction of 12% and evidence that measures of jet concentration and WSS were significantly different depending on the segmentation method.

In [7], the authors evaluated the sensitivity of aneurysm segmentation to DSA kernel reconstruction choice, demonstrating changes in neck width and in resulting CFD-derived hemodynamic parameters. They found that mean ostium surface area was 12.9% larger using a smooth reconstruction kernel compared to a normal or sharp kernel, leading to differences in TAWSS ranging from 6.7% to 36%, although their surface models also included whole-model segmentation differences. In the present study, we controlled all other anatomic variation to ensure hemodynamic differences were caused only by changes at the neck region, resulting in a median ostium reduction of 12% and median and maximum TAWSS differences of 7.4% and 36%, which are comparable in magnitude to Berg et al., suggesting the neck segmentation plays a dominant role in determining hemodynamic conditions among all geometric variation.

In Phase 1b of the Multiple Aneurysm Anatomy Challenge [25], the authors performed CFD for all challenge-submitted segmentations, which varied in terms of both model extent and sac/neck shape, using an inlet flow rate scaled to vessel diameter and under otherwise similar conditions. They reported a maximum variation in aneurysm inflow rate of 46% compared with our 43% and variations in TAWSS of up to 51% compared with our 35%. As expected, interindividual variability in both model extent and sac/neck segmentation appear greater than our errors due to differences in the neck alone, albeit not dramatically, again suggesting that the neck may be the most important source of segmentation variability in aneurysm CFD.

Voß et al. [25] also observed that, for an MCA bifurcation aneurysm, submissions with narrower necks resulted in inflow jets with higher velocity. In the current study, where the neck is the only feature with variation, we do not consistently observe this effect. This phenomenon likely depends on the size of the ostium relative to the aneurysm: taken to extremes, as ostium area approaches 0, we would expect resistance to the incoming jet to increase and inhibit the jet; as neck size approaches the aneurysm sac size, the mechanism for flow concentration and separation ceases to exist; between this range, small changes may promote or inhibit jetting, depending on these geometric features.

As part of a computer experiment designed to quantify changes in hemodynamics in response to aneurysm growth, [26] synthetically modified the sac sizes of N = 88 aneurysms while keeping the neck size fixed. As the ratio (neck size / sac size) decreased, inflow rate to the aneurysm decreased while sac wall shear stress decreased and became more concentrated (higher SCI). Although the current study used modified necks rather than sacs, those results are conceptually consistent with our findings (i.e., smaller necks led to lower inflow rate, lower TAWSS, and increased SCI). Salimi Ashkezari et al. also found that as the aneurysm enlarged (keeping the neck fixed), the inflow jet became more concentrated (larger ICI), while we observed the opposite (slightly decreased ICI), which was consistent with our decrease in Q_{in}; given that their Q_{parent} and A_{ostium} stayed the same size, this implies that A_{in} must have decreased "faster" than Q_{in}, which we suspect may result from inertial differences caused by changing the sac size rather than the neck size.

In [27] the authors compared CFD for paired segmentations generated from 3DRA and less invasive time-resolved CT angiography (so-called 4D-CTA). They ran each 3D/4D pair under two conditions: first, using differing model extents and estimated flow rates (thereby incorporating the "real-world" variability of independently-generated segmentations), and secondly, using matched model extents with patient-specific flow rates. Under the first condition, TAWSS and SPI showed lower correlation compared with the current study (R^2 = 0.59 vs. 0.98, R^2 = 0.13 vs 0.71 respectively), while OSI showed greater correlation (R^2 = 0.64 vs 0.36), suggesting that hemodynamic differences induced by varying model extent with estimated flow rates are generally greater than differences induced by the neck alone. Correlation of TAWSS, OSI, and SPI improved under the second condition where model extent and flow rate were controlled (R^2 = 0.91, 0.79, 0.90 respectively), suggesting that results between 3DRA and 4D-CTA are generally comparable. Both [27] and our study show strong correlation of TAWSS, each with slight biases: Standard watershed segmentation overestimates TAWSS compared with SURGE (likely due to differences in flow resistance to the sac), and 4D-CTA overestimates compared with 3DRA (likely a consequence of differences in inlet diameter and ensuing velocity discrepancies). In the present study, OSI and SPI show lower correlation compared with [27] (R^2 = 0.36

vs 0.79, R^2 = 0.71 vs 0.90), suggesting neck segmentation more-strongly influences flow complexity compared to whole-model segmentation differences introduced by differences in imaging modality.

4.2 Relationship to other sources of uncertainty in aneurysm CFD

In addition to segmentation errors and uncertainties, aneurysm CFD modelling is susceptible to errors and uncertainties arising from choice of inlet/outlet boundary conditions, wall properties, blood properties, and solution strategy [5, 6], so it is important to try and contextualize our findings to studies that have looked at these. Previously, [28] demonstrated that simulated aneurysmal hemodynamics are highly sensitive to numerical solution strategy in N = 12 MCA aneurysms; on average TAWSS was 30% underestimated using a "normal-resolution" strategy compared with a "high-resolution" strategy, although the two showed high correlation (R^2 = 0.97). Similarly, they showed that OSI was underestimated and showed low correlation (R^2 = 0.23), while LSA was generally insensitive to solution strategy. In the present study, the median difference in TAWSS was only -6.2%, suggesting solution strategy likely has a greater impact on WSS-based parameter than neck segmentation errors. Our reported OSI was neither over- nor under-estimated, but also showed low correlation (R^2 = 0.36), while LSA was generally insensitive to segmentation method.

In [29] hemodynamic parameters were compared for simulations using patient-specific flow conditions vs. generalized inflow conditions, resulting in a median difference in TAWSS of 32% and a maximum absolute change of 146%. Compared to our median and maximum absolute differences of 7.4% and 36%, it appears flow rate uncertainty is likely a greater contributor to hemodynamic uncertainty than neck overestimation. For OSI and SPI, Najafi et al. found a median difference of 32% and 71%, compared with our median differences of 25% and 26%. Interestingly, the authors observed stronger correlations for OSI and SPI compared to TAWSS, in contrast to the current study where OSI and SPI showed lower correlation than TAWSS. This could suggest that some parameters may be differentially sensitive to either geometry or flow rate. Alternatively, it is also possible that differences in cohorts may explain this, since the study design of Najafi et al. limited them primarily to sidewall aneurysms that were eventually treated by flow diversion.

As expected, measures associated with flow complexity such as OSI, SCI, SPI, and SBI showed lower correlation and higher maximum errors (81%, 670%, 140%, 160%) than temporally and spatially averaged parameters such as TAWSS or LSA. We emphasize that these maximal discrepancies are not "outliers" in the sense of measurement or experimental error, but rather, demonstrate the divergent effects that neck segmentation can have on hemodynamic parameters; we also note that these extreme discrepancies occurred in only a small number of cases within the current cohort (N = 17), which in turn is only a subset within the full consecutive cohort (N = 60). For SCI, SPI, and SBI, removal of each "outlier" results in stronger correlation (Table 4), which may better represent the "typical" response to changes in neck segmentation. The prevalence of these flow instabilities (SPI ¿ 0.1) was higher in the SURGE vs. Standard group (70% vs 64%), though both were higher than in [30] (34%), which may result from the selection of cases in this limited sample.

4.3 Implications for rupture status/risk assessment

Hemodynamic parameters that are sensitive to small segmentation errors, such as measures of flow complexity, may be less reliable for association studies (especially if the segmentation quality is low or unknown) but may provide opportunity for novel insights into the mechanobiological mechanisms of wall remodelling. Successful clinical utility would require parameters to be robust to intra-patient geometric variation or differences in image quality, but specific enough to differentiate mechanobiologically distinct aneurysms. In a review including 46 studies, Liang et al. [22] ranked geometric and hemodynamic parameters based on the consensus of correlation among published studies. Among 81 geometric and hemodynamic parameters, aspect ratio and size ranked 1st and 2nd, while LSA and TAWSS ranked 3rd and 4th when normalized by sample size. For LSA, a significant positive correlation was found in 9/17 studies, with the remaining showing no significant correlation; for TAWSS, a negative correlation was found in 9/23, and a positive correlation in 2/23, with the remaining insignificant. Liang et al. surmised that the two geometric parameters (aspect ratio and aneurysm size) may have scored highly because their definition is easier to measure and subject to less variation than hemodynamic parameters. Based on our discussion in the previous section, it seems reasonable to suspect that LSA and TAWSS also ranked highly because they are robust to changes in geometry, flow rate, and solution strategy. Put another way, hemodynamic parameters that could be more mechanistically-linked to wall degradation and rupture (e.g., SCI [3] or SBI [4]) might be masked by CFD uncertainties that must be compensated for by large study sizes.

The present study focused on 17/60 cases from a consecutive clinical sample, a subset chosen specifically to assess the sensitivity of hemodynamic parameters to changes in neck segmentation. Most of these cases either occur at a

bifurcation with nearby branches or contain small daughter vessels emerging from the aneurysm or neck itself, as was suggested in [2]. By selecting cases with these geometrical features, we may, for example, be inadvertently selecting cases prone to high-frequency instabilities or other characteristics that may not replicate in a larger population; such differences would be hard to anticipate without the context of a larger study. With that said, within the consecutive sample of 60 consecutive cases, only a small fraction may be affected specifically by neck errors: for TAWSS or LSA, perhaps fewer than 5/60 or 8% could be considered to have "non-negligible" impact of neck segmentation, using an arbitrary threshold of 25% absolute difference. Using the same threshold for measures of flow complexity (OSI, SCI, SPI, SBI), at most 9/60 or 15% would have non-negligible differences induced by the neck alone; increasing the threshold to 50%, this drops to at most 5/60 or 8%. Similarly, based on the velocity contours (as in Fig. 2A and Fig. 2D), as few as 2/60 or 3% appeared be affected by "extreme" neck-induced errors. Our inference that neck overestimation errors may not be prevalent in the aneurysm CFD literature is also consistent with recent work showing an association between aneurysm wall thinning and WSS divergence [31] since one would expect the location and intensity of WSS gradients (e.g., impingement points) to be more sensitive to CFD uncertainties and errors.

4.4 Potential limitations

Neck segmentation introduces variability in hemodynamic parameters among only subset of a given cohort, and as such the prevalence and impact of neck-related errors may be hard to anticipate, especially given variability in image resolution and reconstruction kernel choice [32] or segmentation method [7, 8]. Variability due to neck segmentation may be difficult to identify without manual inspection against high-resolution reference images, but can be overcome, at least to some degree, by the SURGE segmentation method [10]. As that study showed, even with SURGE the necks were still slightly overestimated on average compared to 2D-DSA; however, this does not affect our experimental design since our purpose was to assess the impact of plausible differences in neck geometry on CFD-derived hemodynamics. Our findings are in line with [2], but our approach avoids the tedious and subjective manual-editing process that has previously been necessary to assess the impact of the neck on hemodynamic parameters.

During the initial selection of cases for this study, SURGE was sometimes able to segment small, sac-adjacent branches that could not be captured with Standard watershed, leading us to exclude these cases from this study in order to reduce confounding factors; as such, our results may, if anything, be *underestimating* any differences in hemodynamics between the models when using the SURGE segmentation method generally. This controlled choice in experimental design allowed us to conclusively determine the impact of the neck on hemodynamics; the effect of keeping these small branches and incorporating any changes in boundary conditions is a future area of study. Since patient-specific flow rates were unavailable for these cases, we used a previously-validated methodology for estimating inflow rates; given that our study suggests that many neck-induced errors could, at least in some cases, be of similar order to errors due to flow rate, it may be useful in future works to study potential interactions between anatomical and physiological uncertainties on aneurysm CFD.

5 Conclusion

Errors due to neck segmentation introduce variability to a subset of cases, and these differences are difficult to anticipate and are not necessarily proportional to changes in the ostium area. Neck segmentation may be an important consideration for advancing *patient-specific* hemodynamic modelling, but due to the prevalence and magnitude of typical errors, its impact, on average, is likely smaller than that of flow rate or CFD solution strategy: "extreme" errors may affect as few as 3% of cases, while "non-negligible" errors may affect as much as 15%, depending on the hemodynamic parameter of interest. It should be noted, however, that these conclusions have been drawn from aneurysm models derived from 3DRA, and so may not necessarily extrapolate to those derived from lower-resolution CT or MR angiography.

Variability due to neck segmentation should be acknowledged as a source of uncertainty built in to already-published retrospective CFD studies and should be confronted in future CFD studies via careful inspection of neck regions during segmentation, especially when measures of flow complexity are to be considered or when 3D imaging is performed with low spatial resolution. Ultimately, we encourage CFD practitioners to manually inspect the neck segmentation against an upsampled image gradient (as in [10]) or 2D-DSA where possible.

6 Acknowledgements

This work was supported by a grant to DAS from the Natural Sciences & Engineering Research Council of Canada (RGPIN-2018-04649). DEM acknowledges the generous support of an Ontario Graduate Scholarship and a Barbara & Frank Milligan Graduate Fellowship. VMP acknowledges the generous support from Michael's Family; a JDMI/UHN

Research Leadership Award; and the Schroeder Chair in Advanced Neurovascular Interventions. Computations were performed on the Niagara supercomputer at the SciNet HPC Consortium. SciNet is funded by: the Canada Foundation for Innovation; the Government of Ontario; Ontario Research Fund—Research Excellence; and the University of Toronto.

References

[1] W. Brinjikji et al. "Comparison of 2D Digital Subtraction Angiography and 3D Rotational Angiography in the Evaluation of Dome-to-Neck Ratio". In: *American Journal of Neuroradiology* 30.4 (Apr. 2009), pp. 831–834. DOI: 10.3174/ajnr.A1444.

[2] J. Schneiders et al. "Intracranial Aneurysm Neck Size Overestimation with 3D Rotational Angiography: The Impact on Intra-Aneurysmal Hemodynamics Simulated with Computational Fluid Dynamics". In: *American Journal of Neuroradiology* 34.1 (Jan. 2013), pp. 121–128. DOI: 10.3174/ajnr.A3179.

[3] B. Chung et al. "Identification of Hostile Hemodynamics and Geometries of Cerebral Aneurysms: A Case-Control Study". In: *American Journal of Neuroradiology* 39.10 (Oct. 2018), pp. 1860–1866. DOI: 10.3174/ajnr.A5764.

[4] D. E. MacDonald et al. "Spectral Bandedness in High-Fidelity Computational Fluid Dynamics Predicts Rupture Status in Intracranial Aneurysms". In: *Journal of Biomechanical Engineering* 144.6 (June 2022), p. 061004. DOI: 10.1115/1.4053403.

[5] P. Berg et al. "A review on the reliability of hemodynamic modeling in intracranial aneurysms: why computational fluid dynamics alone cannot solve the equation". In: *Neurosurgical Focus* 47.1 (July 2019), E15. DOI: 10.3171/2019.4.FOCUS19181.

[6] D. A. Steinman and V. M. Pereira. "How patient specific are patient-specific computational models of cerebral aneurysms? An overview of sources of error and variability". In: *Neurosurgical Focus* 47.1 (July 2019), E14. DOI: 10.3171/2019.4.FOCUS19123.

[7] P. Berg et al. "Multiple Aneurysms AnaTomy CHallenge 2018 (MATCH): Phase I: Segmentation". In: *Cardiovascular Engineering and Technology* 9.4 (Dec. 2018), pp. 565–581. DOI: 10.1007/s13239-018-00376-0.

[8] M. Ivantsits et al. "Detection and analysis of cerebral aneurysms based on X-ray rotational angiography - the CADA 2020 challenge". In: *Medical Image Analysis* 77 (Apr. 2022), p. 102333. DOI: 10.1016/j.media.2021.102333.

[9] H. Takao et al. "Comparing Accuracy of Cerebral Aneurysm Size Measurements From Three Routine Investigations: Computed Tomography, Magnetic Resonance Imaging, and Digital Subtraction Angiography". In: *Neurologia medico-chirurgica* 50.10 (2010), pp. 893–899. DOI: 10.2176/nmc.50.893.

[10] D. E. MacDonald et al. "Improving visualization of three-dimensional aneurysm features via segmentation with upsampled resolution and gradient enhancement (SURGE)". In: *Journal of NeuroInterventional Surgery* (June 2022), neurintsurg–2022–018912. DOI: 10.1136/neurintsurg-2022-018912.

[11] M. Attene. "A lightweight approach to repairing digitized polygon meshes". In: *The Visual Computer* 26.11 (Nov. 2010), pp. 1393–1406. DOI: 10.1007/s00371-010-0416-3.

[12] R. Izzo et al. "The Vascular Modeling Toolkit: A Python Library for the Analysis of Tubular Structures in Medical Images". In: *Journal of Open Source Software* 3.25 (May 2018), p. 745. DOI: 10.21105/joss.00745.

[13] M. O. Khan, K. Valen-Sendstad, and D. A. Steinman. "Narrowing the Expertise Gap for Predicting Intracranial Aneurysm Hemodynamics: Impact of Solver Numerics versus Mesh and Time-Step Resolution". In: *American Journal of Neuroradiology* 36.7 (July 2015), pp. 1310–1316. DOI: 10.3174/ajnr.A4263.

[14] S. Hang. "TetGen, a Delaunay-based quality tetrahedral mesh generator". In: *ACM Trans. Math. Softw* 41.2 (2015), p. 11.

[15] P. M. Knupp et al. *The verdict geometric quality library.* Tech. rep. Sandia National Laboratories (SNL), Albuquerque, NM, and Livermore, CA ..., 2006.

[16] C. Chnafa et al. "Errors in power-law estimations of inflow rates for intracranial aneurysm CFD". In: *Journal of Biomechanics* 80 (Oct. 2018), pp. 159–165. DOI: 10.1016/j.jbiomech.2018.09.006.

[17] C. Chnafa et al. "Better Than Nothing: A Rational Approach for Minimizing the Impact of Outflow Strategy on Cerebrovascular Simulations". In: *American Journal of Neuroradiology* 39.2 (Feb. 2018), pp. 337–343. DOI: 10.3174/ajnr.A5484.

[18] M. Mortensen and K. Valen-Sendstad. "Oasis: A high-level/high-performance open source Navier–Stokes solver". In: *Computer Physics Communications* 188 (Mar. 2015), pp. 177–188. DOI: 10.1016/j.cpc.2014.10.026.

[19] F. Mut et al. "Computational hemodynamics framework for the analysis of cerebral aneurysms". In: *International Journal for Numerical Methods in Biomedical Engineering* 27.6 (June 2011), pp. 822–839. DOI: 10.1002/cnm.1424.

[20] H. A. Himburg et al. "Spatial comparison between wall shear stress measures and porcine arterial endothelial permeability". In: *American Journal of Physiology-Heart and Circulatory Physiology* 286.5 (May 2004), H1916–H1922. DOI: 10.1152/ajpheart.00897.2003.

[21] M. O. Khan et al. "On the quantification and visualization of transient periodic instabilities in pulsatile flows". In: *Journal of Biomechanics* 52 (Feb. 2017), pp. 179–182. DOI: 10.1016/j.jbiomech.2016.12.037.

[22] L. Liang et al. "Towards the Clinical utility of CFD for assessment of intracranial aneurysm rupture – a systematic review and novel parameter-ranking tool". In: *Journal of NeuroInterventional Surgery* 11.2 (Feb. 2019), pp. 153–158. DOI: 10.1136/neurintsurg-2018-014246.

[23] J. Xiang et al. "Hemodynamic–morphological discriminant models for intracranial aneurysm rupture remain stable with increasing sample size". In: *Journal of NeuroInterventional Surgery* 8.1 (2014), pp. 104–110. DOI: 10.1136/neurintsurg-2014-011477.

[24] T. Natarajan et al. "On the spectrographic representation of cardiovascular flow instabilities". In: *Journal of Biomechanics* 110 (Sept. 2020), p. 109977. DOI: 10.1016/j.jbiomech.2020.109977.

[25] S. Voß et al. "Multiple Aneurysms AnaTomy CHallenge 2018 (MATCH)—Phase Ib: Effect of morphology on hemodynamics". In: *PLOS ONE* 14.5 (May 2019). Ed. by J. Sznitman, e0216813. DOI: 10.1371/journal.pone.0216813.

[26] S. F. Salimi Ashkezari et al. "Analysis of hemodynamic changes from aneurysm inception to large sizes". In: *International Journal for Numerical Methods in Biomedical Engineering* 37.1 (Jan. 2021). DOI: 10.1002/cnm.3415.

[27] N. M. Cancelliere et al. "4D-CT angiography versus 3D-rotational angiography as the imaging modality for computational fluid dynamics of cerebral aneurysms". In: *Journal of NeuroInterventional Surgery* 12.6 (June 2020), pp. 626–630. DOI: 10.1136/neurintsurg-2019-015389.

[28] K. Valen-Sendstad and D. Steinman. "Mind the Gap: Impact of Computational Fluid Dynamics Solution Strategy on Prediction of Intracranial Aneurysm Hemodynamics and Rupture Status Indicators". In: *American Journal of Neuroradiology* 35.3 (Mar. 2014), pp. 536–543. DOI: 10.3174/ajnr.A3793.

[29] M. Najafi et al. "How patient-specific do internal carotid artery inflow rates need to be for computational fluid dynamics of cerebral aneurysms?" In: *Journal of NeuroInterventional Surgery* 13.5 (May 2021), pp. 459–464. DOI: 10.1136/neurintsurg-2020-015993.

[30] M. Khan et al. "On the prevalence of flow instabilities from high-fidelity computational fluid dynamics of intracranial bifurcation aneurysms". In: *Journal of Biomechanics* 127 (Oct. 2021), p. 110683. DOI: 10.1016/j.jbiomech.2021.110683.

[31] K. Tanaka et al. "A parameter to identify thin-walled regions in aneurysms by CFD". In: *Journal of Neuroendovascular Therapy* 13.6 (2019), pp. 241–249.

[32] P. Berg et al. "Does the DSA reconstruction kernel affect hemodynamic predictions in intracranial aneurysms? An analysis of geometry and blood flow variations". In: *Journal of NeuroInterventional Surgery* 10.3 (Mar. 2018), pp. 290–296. DOI: 10.1136/neurintsurg-2017-012996.